Electron localization function for two-dimensional systems

E. Räsänen,[*] A. Castro,[†] and E. K. U. Gross

Institut für Theoretische Physik, Freie Universität Berlin, Arnimallee 14, D-14195 Berlin, Germany
and European Theoretical Spectroscopy Facility (ETSF)

The concept of the electron localization function (ELF) is extended to two-dimensional (2D) electron systems. We show that the topological properties of the ELF in two dimensions are considerably simpler than in molecules studied previously. We compute the ELF and demonstrate its usefulness for various physical 2D systems focusing on semiconductor quantum dots that effectively correspond to a confined 2D electron gas. The ELF visualizes the shell structure of harmonic quantum dots and provides insight into electron bonding in quantum-dot molecules. In external magnetic fields, the ELF is found to be a useful measure of vorticity when analyzing the properties of quantum-Hall droplets. We show that the current-dependent term in the ELF expression is important in magnetic fields.

I. INTRODUCTION

The study of electron localization is linked to the pursuit of a rigorous systematization of the elusive concept of a chemical bond,[1,2] ubiquitous in quantum chemistry ever since the first attempts of its description.[3] The main point in the concept of electron localization is not where the electrons *are* (or in quantum terms, where the electrons are likely to be), which can be monitored from the electron density, but where the electrons *are localized*.

The concept of localization (and delocalization) arises from Pauli's exclusion principle: two electrons with the same spin cannot occupy the same spatial position. The consequence is the appearance of the *Fermi hole*,[4] a function which determines how the probability of finding an electron at some point diminishes because of the presence of another like-spin electron in its vicinity. In other words, the Fermi hole is that part of the exchange and correlation hole that stems solely from the fermionic nature of the electron and not because of the Coulomb repulsion. Any electron at a given point carries its associated Fermi hole as a counterpart. The localization or delocalization of the electron is equivalent to the localization or delocalization of its Fermi hole.[5,6] Naturally, a localization descriptor should be based on this function or, correspondingly, on the like-spin pair probability function—this will be clarified below. Indeed, the so-called electron localization function[7–10] (ELF) is nothing else than an appropriate renormalization of the Fermi hole curvature.[11,12]

The ELF is large where electrons *pair*. Our intuition in chemistry tells us that electrons should pair forming localized groups in each atomic shell of the inert cores, in the chemical bonds, and in the nonbonding or *lone* pairs. More precisely, the topological properties of a good localization function should partition the space for each group of electrons—also for delocalized groups of electrons such as π systems in conjugated molecules, for which the ELF values should be low. Our understanding of chemistry is founded on the electron pair, a consequence of Pauli's exclusion principle and, more particularly, of the localization of one electron of each spin in a region of space. Accordingly, it is not

surprising that the main purpose of the analysis of the ELF has been to help our intuition of the fundamental chemistry concepts of pairs and bonds.

Due to this focus on the elucidation of the chemical bond, all studies of electron localization functions performed to date have referred to three-dimensional (3D) systems. To our knowledge, no attempts have been made to map the electron localization in two dimensions. However, significant advances in semiconductor technology have enabled the production and manipulation of low-dimensional nanoscale structures. Common examples of these systems are quantum dots (QDs),[13] often also called artificial atoms. The electrons in QDs are confined in the interface of a semiconductor heterostructure, e.g., GaAs/AlGaAs, so that the transverse dimensions controlled by a lateral confinement are considerably larger than the thickness of the QD. In most cases, a two-dimensional (2D) model describes the movement of the electrons with reasonable accuracy. On the other hand, the approximation for the in-plane confinement depends on the QD shape that can be, e.g., circular, rectangular, or ringlike (quantum ring) or consist of several potential minima (quantum-dot molecule). Due to the tunable shape, size, and number of electrons, QDs have emerging applications in fields of quantum computation, and from a theoretical point of view, they are an ideal playground to study many-electron phenomena and test computational methods. Hence, we expect the ELF to be of interest for various QD systems, since it carries valuable information about the electronic structure regardless of the dimensionality.

This paper is organized as follows. In Sec. II, we present a detailed derivation of the ELF in two dimensions, focusing on the definition of the Fermi-hole curvature which is the core of the ELF, and show how the relevant expressions hold compared with the 3D case. We also discuss the topological properties of the ELF in two dimensions. In Sec. III, we briefly present the QD model and our computational scheme based on spin-density-functional theory. In Sec. IV, we provide four examples where the ELF is a useful tool when analyzing the electronic properties of QDs. They include (i) visualization of the shell structure of a parabolic (harmonic) QD, (ii) showing the bondlike interdot electron couplings in QD molecules, (iii) introducing the ELF as a measure of

vorticity in quantum-Hall droplets, and (iv) visualization of vortex localization in high magnetic fields. We also show that the current-dependent term in the ELF (or in the Fermi-hole curvature), which has been neglected in most studies until now, is relevant in order to obtain meaningful results for QDs in magnetic fields. Concluding remarks are given in Sec. V.

II. ELECTRON LOCALIZATION FUNCTION

A. Derivation of the electron localization function in two dimensions

In the following, we go in detail through the mathematical derivation of the ELF. We focus on the differences in the expressions in three and two dimensions, in particular, between the spherical and circular averages and kinetic-energy densities.

We consider the many-electron wave function $\Psi(\mathbf{r}_1\sigma_1, \ldots, \mathbf{r}_N\sigma_N)$, where N is the number of electrons, and $\mathbf{r}$ and σ are the electronic position and spin coordinates, respectively. We point out that Ψ can be either an eigenstate of a static Hamiltonian or an evolving time-dependent state. Nevertheless, we omit the time coordinate in the notation. The necessary ingredients in the derivation of the ELF are the first-order reduced density matrix,[14–16]

$$\Gamma^{(1)}_{\sigma_1\sigma'_1}(\mathbf{r}_1|\mathbf{r}'_1) = N \sum_{\sigma_2,\ldots,\sigma_N} \int d\mathbf{r}_2 \cdots d\mathbf{r}_N$$
$$\times \Psi^*(\mathbf{r}_1\sigma_1, \ldots, \mathbf{r}_N\sigma_N)\Psi(\mathbf{r}'_1\sigma'_1, \ldots, \mathbf{r}_N\sigma_N), \quad (1)$$

and the diagonal of the second-order reduced density matrix,[45]

$$\gamma^{(2)}_{\sigma_1\sigma_2}(\mathbf{r}_1,\mathbf{r}_2) = N(N-1) \sum_{\sigma_3,\ldots,\sigma_N} \int d\mathbf{r}_3 \cdots d\mathbf{r}_N$$
$$\times |\Psi(\mathbf{r}_1\sigma_1, \mathbf{r}_2\sigma_2, \ldots, \mathbf{r}_N\sigma_N)|^2. \quad (2)$$

The diagonal of $\Gamma^{(1)}$ is commonly known as the spin density,

$$n_\sigma(\mathbf{r}) = \Gamma^{(1)}_{\sigma\sigma}(\mathbf{r}|\mathbf{r}), \quad (3)$$

and the total density, $n(\mathbf{r}) = \Sigma_\sigma n_\sigma(\mathbf{r})$, sums over the spin variable. It has an easy interpretation: $n(\mathbf{r})d\mathbf{r}$ is the probability (normalized to N) of finding an electron in a small volume $d\mathbf{r}$ at position $\mathbf{r}$. The *pair probability density* is defined analogously by

$$n^{(2)}(\mathbf{r}_1,\mathbf{r}_2) = \sum_{\sigma_1,\sigma_2} \gamma^{(2)}_{\sigma_1\sigma_2}(\mathbf{r}_1,\mathbf{r}_2) \quad (4)$$

and can be interpreted in the following way: $n^{(2)}(\mathbf{r}_1, \mathbf{r}_2)d\mathbf{r}_1 d\mathbf{r}_2$ is the probability of finding one electron at $\mathbf{r}_1$ and, *simultaneously*, another electron at $\mathbf{r}_2$.

Were the electrons fully independent, this latter probability would just be the product of the electron densities: $n^{(2)}(\mathbf{r}_1,\mathbf{r}_2) = n(\mathbf{r}_1)n(\mathbf{r}_2)$. However, their exchange (fermionic character) and Coulomb interaction reduce the pair probability by a value known as the exchange and correlation hole:

$$n^{(2)}(\mathbf{r}_1,\mathbf{r}_2) = n(\mathbf{r}_1)n(\mathbf{r}_2) + h(\mathbf{r}_1,\mathbf{r}_2). \quad (5)$$

The Fermi hole is the part of $h(\mathbf{r}_1,\mathbf{r}_2)$ which is entirely due to the antisymmetric character of the wave function regardless of the Coulomb interaction. Accordingly, it only appears for like-spin electrons. It is the dominant part at short distances $(\mathbf{r}_2 \rightarrow \mathbf{r}_1)$.

The key function to study the electron localization is the like-spin conditional pair probability function defined as

$$P_\sigma(\mathbf{r}_1,\mathbf{r}_2) \equiv \frac{\gamma^{(2)}_{\sigma\sigma}(\mathbf{r}_1,\mathbf{r}_2)}{n_\sigma(\mathbf{r}_1)}. \quad (6)$$

The physical meaning of this function is the following. It gives the probability of finding one σ-spin electron at $\mathbf{r}_2$ knowing with certainty that another σ-spin electron is at $\mathbf{r}_1$. The question is now how probable it is to find one like-spin electron in the vicinity of the first reference one. For this purpose, it is useful to define a conditional pair probability function at a distance s via a spherical (in three dimensions) or circular (in two dimensions) average. Here, we deal with the latter case,

$$p_\sigma(\mathbf{r}_1,s) = \frac{1}{2\pi}\int_0^{2\pi} d\theta P_\sigma(\mathbf{r}_1,\mathbf{r}_1 + s\hat{\mathbf{u}}_\theta), \quad (7)$$

where $\hat{\mathbf{u}}_\theta = \cos\theta\hat{\mathbf{x}}_1 + \sin\theta\hat{\mathbf{x}}_2$. Since we are particularly interested in the behavior of $p_\sigma(\mathbf{r},s)$ at small s, we need to perform Taylor expansions,

$$\Psi[\mathbf{r}_1\sigma,(\mathbf{r}_1 + s\hat{\mathbf{u}}_\theta)\sigma, \ldots, \mathbf{r}_N\sigma_N]$$
$$= s(\hat{\mathbf{u}}_\theta \cdot \nabla_2)\Psi(\mathbf{r}_1\sigma,\mathbf{r}_2\sigma, \ldots, \mathbf{r}_N\sigma_N)_{\mathbf{r}_2=\mathbf{r}_1} + \mathcal{O}(s^2), \quad (8)$$

where ∇_2 is the gradient with respect to the second electron variable in Ψ. The s^0 term is absent due to Pauli's exclusion principle. We now take the square,

$$|\Psi[\mathbf{r}_1\sigma,(\mathbf{r}_1 + s\hat{\mathbf{u}}_\theta)\sigma, \ldots, \mathbf{r}_N\sigma_N]|^2$$
$$= s^2|(\hat{\mathbf{u}}_\theta \cdot \nabla_2)\Psi(\mathbf{r}_1\sigma,\mathbf{r}_2\sigma, \ldots, \mathbf{r}_N\sigma_N)_{\mathbf{r}_2=\mathbf{r}_1}|^2 + \mathcal{O}(s^3)$$
$$= s^2 \sum_{i,j=1}^2 c_i^* c_j u_i(\theta)u_j(\theta) + \mathcal{O}(s^3), \quad (9)$$

where

$$c_i = (\hat{\mathbf{x}}_i \cdot \nabla_2)\Psi(\mathbf{r}_1\sigma,\mathbf{r}_2\sigma, \ldots, \mathbf{r}_N\sigma_N)_{\mathbf{r}_2=\mathbf{r}_1}, \quad (10)$$

with $i=1,2$. The circular average is

$$\frac{1}{2\pi}\int_0^{2\pi} d\theta|\Psi[\mathbf{r}_1\sigma,(\mathbf{r}_1 + s\hat{\mathbf{u}}_\theta)\sigma, \ldots, \mathbf{r}_N\sigma_N]|^2$$
$$= s^2 \sum_{i,j=1}^2 c_i^* c_j \frac{1}{2\pi}\int_0^{2\pi} d\theta u_i(\theta)u_j(\theta)$$
$$= \frac{1}{2}s^2 \sum_{i=1}^2 |c_i|^2 + \mathcal{O}(s^3)$$
$$= \frac{1}{4}s^2\nabla_2^2|\Psi(\mathbf{r}_1\sigma,\mathbf{r}_2\sigma, \ldots, \mathbf{r}_N\sigma_N)|^2_{\mathbf{r}_2=\mathbf{r}_1} + \mathcal{O}(s^3). \quad (11)$$

This expression may then be used in combination with Eqs. (2), (6), and (7) to obtain

$$p_\sigma(\mathbf{r}_1, s) = \frac{1}{2} s^2 C_\sigma(\mathbf{r}_1) + \mathcal{O}(s^3), \qquad (12)$$

$$C_\sigma(\mathbf{r}_1) = \frac{1}{2} \frac{\nabla_2^2 \gamma_{\sigma\sigma}^{(2)}(\mathbf{r}_1, \mathbf{r}_2)_{\mathbf{r}_2 = \mathbf{r}_1}}{n_\sigma(\mathbf{r}_1)}. \qquad (13)$$

These equations are similar to the ones obtained in the 3D case; in fact, they are the same *except* for the factor $1/2$ in Eq. (12), which is $1/3$ in three dimensions. The function $C_\sigma(\mathbf{r})$ satisfies exactly the same Eq. (13) in two and three dimensions. This is the function that measures the *local* like-spin pair probability, is an inverse measure of electron localization, and is the function used to define the ELF. We should also note that $\nabla_2^2 \gamma_{\sigma\sigma}^{(2)}(\mathbf{r}_1, \mathbf{r}_2)_{\mathbf{r}_2 = \mathbf{r}_1}$ is the Fermi-hole curvature as defined by Dobson.[11] Other definitions, equivalent regarding the information that they contain, are also possible.[17]

We conclude that the expressions that define the ELF do not change significantly from three to two dimensions. The function $C_\sigma(\mathbf{r})$ alone does not reveal the localization explicitly. For that purpose, one needs to perform the following renormalization, which defines the ELF as[46]

$$\mathrm{ELF}_\sigma(\mathbf{r}) = \frac{1}{1 + \{C_\sigma(\mathbf{r})/C_\sigma^{\mathrm{HEG}}[n_\sigma(\mathbf{r})]\}^2}, \qquad (14)$$

where $C_\sigma^{\mathrm{HEG}}[n_\sigma(\mathbf{r})]$ is the value of the C_σ function for the homogeneous electron gas of (constant) spin densities $n_\sigma(\mathbf{r})$. Analogously to the 3D case, the expression for C_σ^{HEG} in two dimensions is the kinetic-energy density,

$$C_\sigma^{\mathrm{HEG}}[n_\sigma] = \tau_\sigma[n_\sigma] = 2\pi n_\sigma. \qquad (15)$$

In terms of the total density n and the polarization (often also called magnetization) $\zeta = (n_\uparrow - n_\downarrow)/n$, the expression immediately yields

$$C_\sigma^{\mathrm{HEG}}[n, \zeta] = \frac{\pi}{2}(1 + \zeta^2)n \qquad (16)$$

for the total kinetic-energy density.

The above definition of C_σ is completely general but requires the diagonal of the second-order reduced density matrix, which is a fairly complex and often unmanageable object. In most cases, however, a further approximation is taken by assuming that Ψ is a single-determinantal wave function. In practice, this means that one uses the Hartree-Fock approximation, therefore neglecting the effect of correlations in the ELF, or one uses density-functional theory (DFT) (see below) and calculates the ELF of the noninteracting auxiliary Kohn-Sham (KS) system. Both possibilities are in principle unsatisfactory, but experience has demonstrated that the results are usually unaffected despite a notable mathematical simplification (see Ref. 19 for the detailed steps). If Ψ is formed by the set of KS orbitals $\{\varphi_{i\uparrow}\}_{i=1}^{N_\uparrow}$ and $\{\varphi_{i\downarrow}\}_{i=1}^{N_\downarrow}$ ($N_\uparrow + N_\downarrow = N$) within the spin-DFT (SDFT), one finds

$$C_\sigma(\mathbf{r}) = \tau_\sigma(\mathbf{r}) - \frac{1}{4} \frac{[\nabla n_\sigma(\mathbf{r})]^2}{n_\sigma(\mathbf{r})} - \frac{\mathbf{j}_{p,\sigma}^2(\mathbf{r})}{n_\sigma(\mathbf{r})}, \qquad (17)$$

where $n_\sigma(\mathbf{r}) = \Sigma_{i=1}^{N_\sigma} |\varphi_{i\sigma}(\mathbf{r})|^2$ is the spin density [cf. Eq. (3)], τ_σ is the kinetic-energy density given by

$$\tau_\sigma(\mathbf{r}) = \sum_{i=1}^{N_\sigma} |\nabla \varphi_{i\sigma}(\mathbf{r})|^2, \qquad (18)$$

and $\mathbf{j}_{p,\sigma}$ is the spin-resolved paramagnetic current density,

$$\mathbf{j}_{p,\sigma}(\mathbf{r}) = \frac{i}{2} \sum_{i=1}^{N_\sigma} \{[\nabla \varphi_{i\sigma}^*(\mathbf{r})]\varphi_{i\sigma}(\mathbf{r}) - \varphi_{i\sigma}^*(\mathbf{r}) \nabla \varphi_{i\sigma}(\mathbf{r})\}. \qquad (19)$$

Here, we point out that most ELF calculations refer to closed-shell molecules (or finite systems in general) in their ground state and in the absence of magnetic fields or the spin-orbit coupling. In those cases, real wave functions can be assumed and the current term in Eq. (17) is absent. In Secs. IV C and IV D, we note the importance of the current term, which is needed in the ELF also during time-dependent processes.[20,21]

B. Topological properties

The basis for the topological investigation of the ELF was established by Silvi and Savin.[8] The information contained in the ELF is extracted with the help of some basic concepts borrowed from the theory of dynamical systems.[22,23] The ELF is a scalar continuous function bounded between 0 and 1, and one should look at its gradient field, which in turn defines the set of attractors—roughly speaking, the maxima of the ELF. The important concept is then that of a *basin* of each attractor—the set of points for which that attractor is the ω limit. In chemistry, each basin is then identified either as a core basin (it contains a nucleus) or as a valence basin. The latter ones are then classified according to the number of core basins that they have a frontier with: if they have only one neighbor core, they are called monosynaptic; if they have more than one (disynaptic, trisynaptic, etc.), they are *bonds*. The absence of real nuclei in the 2D models makes this distinction not relevant. However, the division of space into localization basins is still pertinent: the basins give us information about the *groups* of electrons; exchange of electrons is more unlikely between different basins than inside them. In three dimensions, the attractors can then be single points in the absence of special symmetries, ring-shaped lines of attractors around a symmetry axis, or spheres around isolated atoms. In two dimensions, obviously, the topology simplifies and we can only find, besides point attractors, ring attractors for cylindrically symmetrical problems.

III. QUANTUM-DOT MODEL

We study the ELF in 2D QDs restricted to the xy plane. The system is described by an effective-mass N-electron Hamiltonian,

$$H = \sum_{i=1}^{N} \left[\frac{\left(\mathbf{p}_i + \frac{1}{c} \mathbf{A}_i \right)^2}{2m^*} + V_{\text{ext}}(\mathbf{r}_i) + E_{Z,i} \right] + \sum_{i<j} \frac{1}{\epsilon^* |\mathbf{r}_i - \mathbf{r}_j|},$$

(20)

where $\mathbf{A}$ is the external vector potential (in symmetric gauge) of the homogeneous magnetic field $\mathbf{B} = B_0 \hat{z}$ perpendicular to the plane, $V_{\text{ext}}(\mathbf{r})$ is the external confining potential in the xy plane (see below), and $E_Z = g^* \mu_B s_z B_0$ is the Zeeman energy. We apply the conventional effective-mass approximation with the material parameters for GaAs: the effective mass $m^* = 0.067$, the dielectric constant $\epsilon^* = 12.4$, and the gyromagnetic ratio $g^* = -0.44$.

We solve the ground-state problem associated with the N-electron Hamiltonian in Eq. (20) by applying the SDFT in the collinear-spin representation. The KS states, needed in Eqs. (17)–(19) for computing the ELF as defined in Eq. (14), are solved from the KS equation

$$\left[\frac{\left(\mathbf{p} + \frac{1}{c} \mathbf{A} \right)^2}{2m^*} + V_{\text{KS}}^{\sigma}(\mathbf{r}) \right] \varphi_{i\sigma}(\mathbf{r}) = \epsilon_{i\sigma} \varphi_{i\sigma}(\mathbf{r}),$$

(21)

where the KS potential $V_{\text{KS}}^{\sigma}(\mathbf{r})$ is a sum of the external confining potential, the Hartree potential, and the exchange-correlation potential given by $V_{\text{xc}}^{\sigma}(\mathbf{r}) = \delta E_{\text{xc}}[n^{\uparrow}, n^{\downarrow}] / \delta n^{\sigma}(\mathbf{r})$. To approximate the exchange-correlation energy E_{xc}, we use the local spin-density approximation (LSDA) with a parametrization provided by Attaccalite and co-workers.[24] In QD systems, the SDFT scheme together with the LSDA leads to good numerical accuracy in comparison with quantum Monte Carlo calculations even in relatively high magnetic fields.[25,26] We also point out that the local-vorticity approximation within the current SDFT (Ref. 27) does not lead to a considerable improvement over the SDFT results.[25] In the numerical calculations, we apply the real-space OCTOPUS code.[28]

IV. EXAMPLES

A. Shell structure

First, we examine the ELF in parabolic QDs at zero magnetic field ($B = 0$). Thus, we choose the external confining potential in Eq. (20) as $V_{\text{ext}}(r) = \omega_0^2 r^2 / 2$, where we set the confinement strength to $\omega_0 = 0.421\,68$ a.u. = 5 meV. The system is a 2D harmonic oscillator with single-electron eigenenergies $\epsilon_{nl} = (2n + |l| + 1)\omega_0$, where $n = 0, 1, 2, \ldots$ is the radial and $l = 0, \pm 1, \pm 2, \ldots$ is the azimuthal quantum number. The corresponding shell structure has been experimentally well depicted in the additional energies of a double-barrier GaAs QD.[29] Further details in the measured addition energies resulting from the electron-electron interaction, such as Hund's rule-type of behavior, have been theoretically verified in numerous studies employing, e.g., SDFT.[30–32]

Figure 1 shows the ELF (red solid lines) and the corresponding electron densities (blue dashed lines) when $N = 6$, 12, 20, 30, 42, and 56. In QDs, these "magic" electron numbers correspond to the first closed-shell configurations when
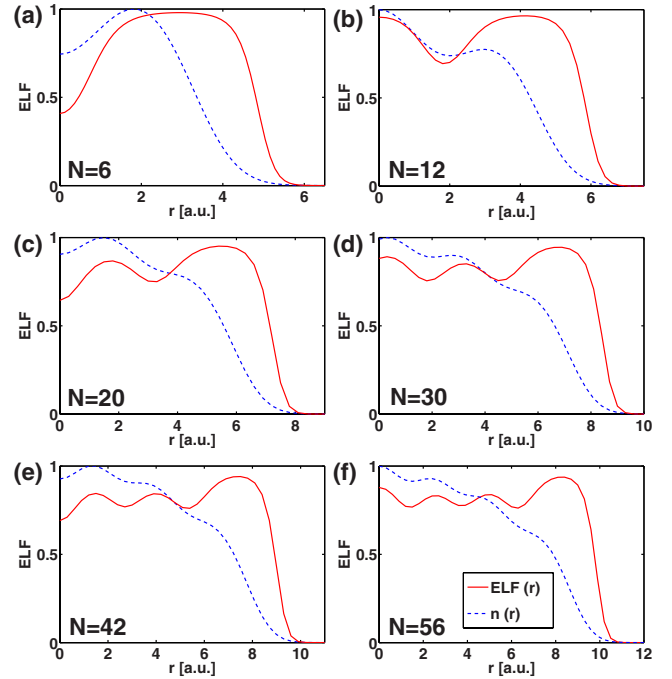

FIG. 1. (Color online) ELF (red solid lines) with the corresponding electron densities (blue dashed lines) for two-dimensional closed-shell quantum dots. The maximum-density values are scaled to 1.

$N > 2$. The shell structure is visualized clearly by the ELF. We note, however, that the local maxima in the ELF do not directly correspond to the filled energy shells. Instead, each peak can be associated with a doubly occupied single-electron state on the *highest* energy shell. This means that the probability of electron localization is highest close to the Fermi level. For example, in a 12-electron QD shown in Fig. 1(b), the highest energy shell has six electrons with $l = 0, \pm 2$, leading to distinctive peaks in the ELF at the center (corresponding to $l = 0$) and at $r \sim 4$ (corresponding to $l = \pm 2$). Nevertheless, in this system, the number of energy shells is equal to the number of extrema in the ELF. As expected, the variation between the extrema decreases as a function of N, since the highest shell becomes relatively less dominant. As seen in Fig. 1, the shell structure is visible also in the electron density $n(r)$, but it is less clear than in the ELF, especially at large electron numbers where the structure is barely visible. The ELF instead provides an unambiguous visualization of the shell structure, which is well plausible from its physical nature discussed in Secs. I and II.

B. Quantum-dot molecules

The applicability of the ELF to visualize pairs and bonds in molecules immediately suggests to use the ELF for the 2D counterparts commonly known as QD molecules (QDMs). Since the spin-qubit proposal of Loss and DeVincenzo[33] in 1998, coupled QD systems have attracted wide interest both experimentally[34] and theoretically,[35] particularly in terms of charge and spin manipulation. Following the standard QDM definition, we write the external confining potential as
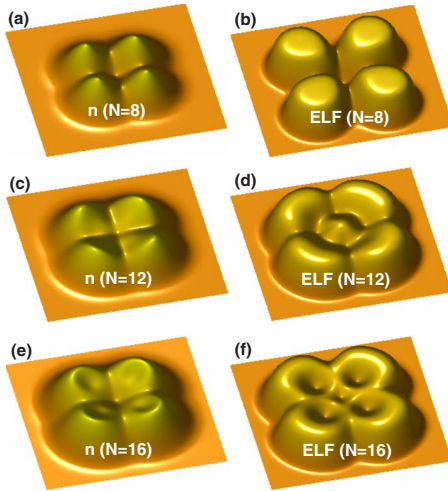
FIG. 2. (Color online) Ground-state total densities and ELFs for four-minima quantum-dot molecules having 8, 12, and 16 electrons, respectively. The total spin $S=0$ in all the cases.

$$V_{\text{ext}}(\mathbf{r}) = \frac{1}{2}\omega_0^2 \min\left[\sum_j^M (\mathbf{r} - \mathbf{r}_j)^2\right], \qquad (22)$$

where M is the number of potential minima located at $\mathbf{r}_j = (x_j, y_j)$. The case of $M=1$, $\mathbf{r}_j = (0,0)$ is equal to a single harmonic QD considered above. Here, we set $M=4$ and $\mathbf{r}_j = (\pm\sqrt{2}, \pm\sqrt{2})$ with $\omega_0 = 0.5$ a.u. This corresponds to a square-symmetric QDM with four minima.[36] Now, Fig. 2 shows the result of our SDFT calculations for the total densities and ELFs when $N=8$ [(a) and (b)], $N=12$ [(c) and (d)], and $N=16$ [(e) and (f)], respectively. The ground-state total spin $S=0$ in all the cases shown. The densities of $N=8$ and $N=12$ QDMs look very similar with four distinctive peaks, whereas the $N=16$ QDM shows more structure around the density maxima. However, the ELFs of these QDMs are very different from each other, having four maxima with one (local) minimum ($N=8$), five maxima with four minima ($N=12$), and four maxima with five minima ($N=16$). Despite the fact that the concept of chemical bonding seems less meaningful in systems where the confining potential is fixed (such as in 2D QD systems), the central "basin" (see Sec. II B) in Fig. 2(d), for example, is very informative: there is pronounced localization at the center, where the confining potential actually has a repulsive cusp. Furthermore, this ground-state property is not at all visible in the bare electron density shown in Fig. 2(c). Therefore, we find that the ELF reveals features in the electronic structure of QDMs which are absent in the electron density—a fact also demonstrated in three dimensions.

C. Maximum-density droplet

Next, we perform our analysis of the 2D ELF for nonzero external magnetic fields ($B > 0$). As the first example, we consider a maximum-density droplet[37,38] (MDD) of a single parabolic QD. The MDD is a fully polarized ($S = N/2$) state, where the electrons have consecutive angular momenta from
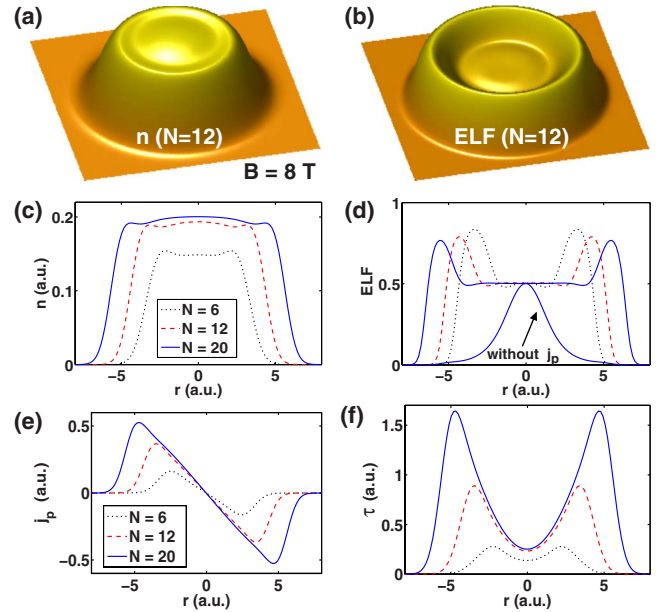

FIG. 3. (Color online) [(a) and (b)] Electron density and ELF of the maximum-density droplet in a 12-electron quantum dot. [(c) and (d)] Intersections of (a) and (b) together with the results for $N=6$ and $N=20$ quantum dots. [(e) and (f)] Paramagnetic current densities and the kinetic-energy densities of the maximum-density-droplet states, respectively.

$l=0$ to $l=-N+1$. Each electron is accompanied by a so-called *Pauli vortex* which corresponds to a change of 2π in the phase of the many-electron wave function. Hence, the MDD state is a unique finite-size counterpart of the filling factor $\nu=1$ quantum-Hall state of the uniform 2D electron gas. Figures 3(a) and 3(b) show the electron density and the ELF of the MDD state in a 12-electron parabolic QD at $B = 8$ T. The MDD density has the well-known flat shape,[37,38] whereas the ELF is characterized by a flat interior and localization around the edge of the QD. Intersections of the density and the ELF are plotted in Figs. 3(c) and 3(d) (red dashed lines), together with the results for 6- and 20-electron QDs at $B=6$ and 8 T, respectively. Interestingly, the values of the ELF are very close to $1/2$ in the interior of the MDDs. Thus, from Eq. (14), we find $C_\sigma(\mathbf{r}) \approx C_\sigma^{\text{HEG}}(\mathbf{r})$ in this regime, i.e., the kinetic-energy density of the uniform 2D electron gas. The result suggests that the localization of electrons and vortices compensate each other, which is well plausible considering the $\nu=1$ character of the MDD state. We may thus expect that at higher magnetic fields, corresponding to the fractional quantum-Hall regime ($\nu < 1$), ELF values below $1/2$ can be found at positions of high vorticity.

Figure 3(d) also shows the ELF of the $N=20$ QD calculated without the current-density term j_p in Eq. (17). That curve equals to the full ELF at $r=0$ where the current density is zero but decays exponentially at larger r. Obviously, that result does not capture the correct behavior of the MDD state. The dramatic difference demonstrates the importance of the current-density dependence in the ELF expression, already at relatively moderate magnetic fields. In Fig. 3(e), we plot j_p which increases linearly due to the successive
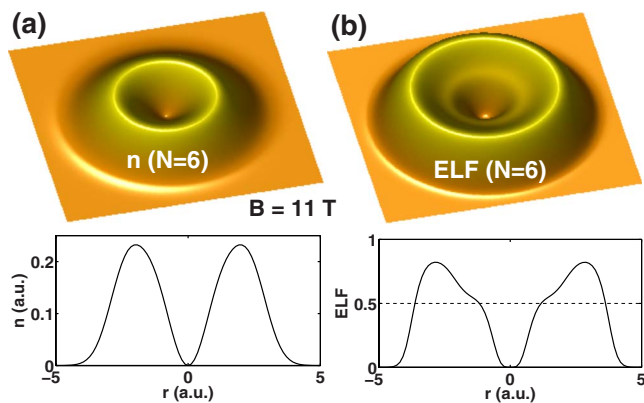
FIG. 4. (Color online) (a) Electron density and the (b) ELF of a single-vortex solution in a six-electron parabolic quantum dot at $B=11$ T. The lower panel shows middle intersections of the figures in the upper panel.
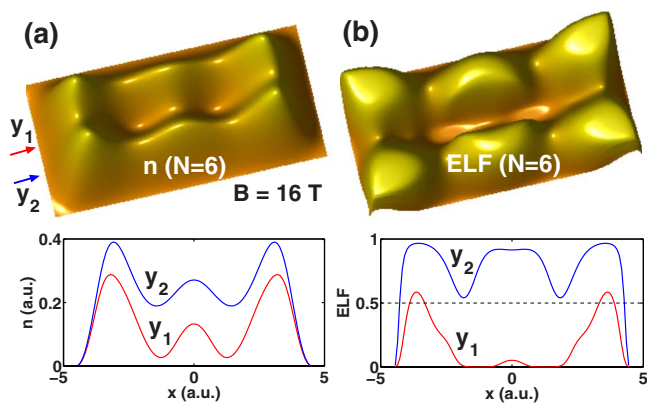

FIG. 5. (Color online) (a) Electron density and (b) the ELF of a two-vortex solution in a six-electron rectangular quantum dot at $B=16$ T. The lower panel shows intersections of the upper figures at y_1 and y_2, marked in the upper right figure.

increase in the angular momenta of the KS states in the MDD (see above).

D. Vortex structures

Increasing the magnetic field above the MDD limit at $\nu=1$, which, as seen above, corresponds to ELF=1/2, leads to localization of vortices. Depending on the QD geometry, the vortices may form clusters[39–42] or merge together yielding multiple phase quantization.[43] In Fig. 4, we show the electron density and the ELF of a single-vortex solution in a six-electron parabolic QD at $B=11$ T. In this case, the vortex is localized at the center and directly visible as a hole in the density. As expected, the ELF shows a similar structure. The ELF has a bump with a value of $\sim 1/2$, located between the center and the edge of the QD. This region can be interpreted to have, on average, a local balance between electrons and (Pauli) vortices, and it separates the localized vortex (ELF=0) from the edge having high electron localization (ELF ≈ 0.8).

Increasing the magnetic field further leads to the formation of more vortices. Figure 5 shows a two-vortex structure in a six-electron rectangular (hard-wall) QD at $B=16$ T. The system has been studied in detail in Refs. 41 and 44. Again, the vortices are seen as zeros in the ELF, whereas the density is *not* exactly zero at these positions. Actually, the numerically exact density at the vortices is even further above zero than the SDFT density due to the multiconfigurational nature of the many-electron wave function.[41] Nevertheless, the ELF=0 result at the vortex positions is plausible, reflecting again the difference between the probable *location* (density) and the *localization* (ELF) of the electrons as discussed in Sec. I. Along the edge of the QD, the ELF in Fig. 5(b) shows six clear peaks with maximum values close to 1, separated by local minima where ELF $\sim 1/2$. Thus, in this QD, the ELF reveals the Wigner crystallization, i.e., localization of electrons around their classical positions which are determined by the geometry of the system. This effect is considerably less pronounced in the electron density shown in Fig. 5(a).

V. CONCLUDING REMARKS

The electronic structure of a many-electron system is fully characterized by its many-body wave function. In order to acquire an intuitive visual understanding of the system, however, we must look at simpler objects—integrated magnitudes such as the electronic density, which lives in a lower-dimensional space. Unfortunately, the density does not fully reveal all the intricacies of the electronic structure, even if we know that it contains all the information.

In the past, the ELF has proven to be a useful companion to the density in the task of providing us with insightful intuition on the electronic structure of molecules. In this work, we have defined the ELF in two dimensions, and we have demonstrated that its visualization, in addition to that of the density, helps us understand the electronic structure of 2D systems such as semiconductor quantum dots. We have shown the usefulness of the ELF to visualize the shell structure, as well as the bondlike features in coupled systems. In particular, we have found that in magnetic fields, the ELF can be used as a measure of vorticity, revealing the local relation between the localization of electrons and vortices in the system. In this context, we have shown that the current-dependent term, which has been neglected in previous 3D studies, has a major contribution to the ELF in magnetic fields. We expect that alongside the rapid technological developments in the fabrication and manipulation of low-dimensional systems, the ELF will prove to be a universally applicable theoretical tool to obtain detailed information of both static and dynamic many-particle properties.

ACKNOWLEDGMENTS

*esa@physik.fu-berlin.de

†alberto@physik.fu-berlin.de

[1] L. Pauling, *The Nature of the Chemical Bond* (Cornell University Press, Ithaca, 1948).

[2] G. N. Lewis, *Valence and Structure of Atoms and Molecules* (Dover, New York, 1966).

[3] G. N. Lewis, J. Am. Chem. Soc. **38**, 762 (1916).

[4] P.-O. Löwdin, Adv. Chem. Phys. **2**, 207 (1959).

[5] R. F. W. Bader, A. Streitwieser, A. Neuhaus, K. E. Laidig, and P. Speers, J. Am. Chem. Soc. **118**, 4959 (1996).

[6] F. F. W. Bader, S. Johnson, T.-H. Tang, and P. L. A. Popelier, J. Phys. Chem. **100**, 15398 (1996).

[7] A. D. Becke and K. E. Edgecombe, J. Chem. Phys. **92**, 5397 (1990).

[8] B. Silvi and A. Savin, Nature (London) **371**, 683 (1994).

[9] A. Savin, R. Nesper, S. Wengert, and T. F. Fässler, Angew. Chem., Int. Ed. Engl. **36**, 1808 (1997).

[10] B. Silvi, I. Fourré, and M. E. Alikhani, Monatsch. Chem. **136**, 855 (2005).

[11] J. F. Dobson, J. Chem. Phys. **94**, 4328 (1991).

[12] J. F. Dobson, J. Chem. Phys. **98**, 8870 (1993).

[13] For reviews, see L. Jacak, P. Hawrylak, and A. Wójs, *Quantum Dots* (Springer, Berlin, 1998); L. P. Kouwenhoven, D. G. Austing, and S. Tarucha, Rep. Prog. Phys. **64**, 701 (2001); S. M. Reimann and M. Manninen, Rev. Mod. Phys. **74**, 1283 (2002).

[14] P.-O. Löwdin, Phys. Rev. **97**, 1474 (1955).

[15] R. McWeeny, Rev. Mod. Phys. **32**, 335 (1960).

[16] R. McWeeny, *Methods of Molecular Quantum Mechanics* (Academic, New York, 1989).

[17] H. Stoll, E. Golka, and H. Preuss, Theor. Chim. Acta **55**, 29 (1980).

[18] M. Kohout, Int. J. Quantum Chem. **97**, 651 (2004).

[19] T. Burnus, MSc thesis, Freie Universität Berlin, 2004.

[20] T. Burnus, M. A. L. Marques, and E. K. U. Gross, Phys. Rev. A **71**, 010501(R) (2005).

[21] A. Castro, T. Burnus, M. A. L. Marques, and E. K. U. Gross, in *Analysis and Control of Ultrafast Photoinduced Reactions*, Springer Series in Chemical Physics Vol. 87, edited by O. Kühn and L. Wöste (Springer, Heidelberg, 2007), Chap. 6.5, pp. 555–576.

[22] R. H. Abraham and C. D. Shaw, *Dynamics: The Geometry of Behavior* (Addison-Wesley, Reading, MA, 1992).

[23] R. H. Abraham and J. E. Marsden, *Foundations of Mechanics* (Addison-Wesley, Reading, MA, 1994).

[24] C. Attaccalite, S. Moroni, P. Gori-Giorgi, and G. B. Bachelet, Phys. Rev. Lett. **88**, 256601 (2002).

[25] H. Saarikoski, E. Räsänen, S. Siljamäki, A. Harju, M. J. Puska, and R. M. Nieminen, Phys. Rev. B **67**, 205327 (2003).

[26] E. Räsänen, H. Saarikoski, A. Harju, M. Ciorga, and A. Sachrajda, Phys. Rev. B **77**, 041302(R) (2008).

[27] G. Vignale and M. Rasolt, Phys. Rev. Lett. **59**, 2360 (1987).

[28] A. Castro, H. Appel, M. Oliveira, C. A. Rozzi, X. Andrade, F. Lorenzen, M. A. L. Marques, E. K. U. Gross, and A. Rubio, Phys. Status Solidi B **243**, 2465 (2006).

[29] S. Tarucha, D. G. Austing, T. Honda, R. J. van der Hage, and L. P. Kouwenhoven, Phys. Rev. Lett. **77**, 3613 (1996).

[30] K. Hirose and N. S. Wingreen, Phys. Rev. B **59**, 4604 (1999).

[31] S. M. Reimann, M. Koskinen, J. Kolehmainen, M. Manninen, D. G. Austing, and S. Tarucha, Eur. Phys. J. D **9**, 105 (1999).

[32] M. Aichinger and E. Räsänen, Phys. Rev. B **71**, 165302 (2005).

[33] D. Loss and D. P. DiVincenzo, Phys. Rev. A **57**, 120 (1998).

[34] For recent experiments, see, e. g., J. R. Petta, A. C. Johnson, J. M. Taylor, E. A. Laird, A. Yacoby, M. D. Lukin, C. M. Marcus, M. P. Hanson, and A. C. Gossard, Science **309**, 2180 (2005); J. Gorman, D. G. Hasko, and D. A. Williams, Phys. Rev. Lett. **95**, 090502 (2005).

[35] See, e. g., A. Wensauer, O. Steffens, M. Suhrke, and U. Rössler, Phys. Rev. B **62**, 2605 (2000); A. Harju, S. Siljamäki, and R. M. Nieminen, Phys. Rev. Lett. **88**, 226804 (2002); M. Forre, J. P. Hansen, V. Popsueva, and A. Dubois, Phys. Rev. B **74**, 165304 (2006).

[36] M. Helle, A. Harju, and R. M. Nieminen, Phys. Rev. B **72**, 205329 (2005).

[37] A. H. MacDonald, S. R. Eric Yang, and M. D. Johnson, Aust. J. Phys. **46**, 345 (1993).

[38] T. H. Oosterkamp, J. W. Janssen, L. P. Kouwenhoven, D. G. Austing, T. Honda, and S. Tarucha, Phys. Rev. Lett. **82**, 2931 (1999).

[39] H. Saarikoski, A. Harju, M. J. Puska, and R. M. Nieminen, Phys. Rev. Lett. **93**, 116802 (2004).

[40] M. Manninen, S. M. Reimann, M. Koskinen, Y. Yu, and M. Toreblad, Phys. Rev. Lett. **94**, 106405 (2005).

[41] H. Saarikoski, S. M. Reimann, E. Räsänen, A. Harju, and M. J. Puska, Phys. Rev. B **71**, 035421 (2005).

[42] M. B. Tavernier, E. Anisimovas, and F. M. Peeters, Phys. Rev. B **74**, 125305 (2006).

[43] E. Räsänen, H. Saarikoski, Y. Yu, A. Harju, M. J. Puska, and S. M. Reimann, Phys. Rev. B **73**, 235324 (2006).

[44] E. Räsänen, A. Harju, M. J. Puska, and R. M. Nieminen, Phys. Rev. B **69**, 165309 (2004).

[45] Note that we follow the convention of McWeeny (Ref. 15), who used an $N(N-1)$ factor for the second-order density matrix rather than the $N(N-1)/2$ factor used by Löwdin (Ref. 14).

[46] We point out that an alternative route to define a localization function has been described by Kohout (Ref. 18). For one-determinantal wave functions, Kohout's *electron localizability index* reduces to the ELF expression, with no need of an *ad hoc* renormalization.